Mass measurement of graphene using quartz crystal microbalances

Dolleman, Robin J.; Hsu, Mick; Vollebregt, Sten; Sader, John E.; Van Der Zant, Herre S.J.; Steeneken, Peter G.; Ghatkesar, Murali K.

DOI
10.1063/1.5111086

Publication date
2019

Document Version
Final published version

Published in
Applied Physics Letters

Applied Physics Letters

Mass measurement of graphene using quartz crystal microbalances

Cite as: Appl. Phys. Lett. **115**, 053102 (2019); https://doi.org/10.1063/1.5111086
Submitted: 23 May 2019 . Accepted: 05 July 2019 . Published Online: 29 July 2019

Robin J. Dolleman, Mick Hsu, Sten Vollebregt, et al.

Applied Physics Letters ARTICLE scitation.org/journal/apl

Mass measurement of graphene using quartz crystal microbalances

Cite as: Appl. Phys. Lett. **115**, 053102 (2019); doi: 10.1063/1.5111086
Submitted: 23 May 2019 · Accepted: 5 July 2019 ·
Published Online: 29 July 2019

Robin J. Dolleman,[1,a),b)] Mick Hsu,[1] Sten Vollebregt,[2] John E. Sader,[3] Herre S. J. van der Zant,[1] Peter G. Steeneken,[1,4] and Murali K. Ghatkesar[4,c)]

AFFILIATIONS

[1]Kavli Institute of Nanoscience, Delft University of Technology, Lorentzweg 1, 2628 CJ Delft, The Netherlands
[2]Department of Microelectronics, Delft University of Technology, Feldmannweg 17, 2628CT Delft, The Netherlands
[3]ARC Centre of Excellence in Exciton Science, School of Mathematics and Statistics, The University of Melbourne, Victoria 3010, Australia
[4]Department of Precision and Microsystems Engineering, Delft University of Technology, Mekelweg 2, 2628 CD Delft, The Netherlands

[a)]**Current address:** 2nd Institute of Physics, RWTH Aachen University, 52074 Aachen, Germany.
[b)]**Electronic mail:** dolleman@physik.rwth-aachen.de
[c)]M.K.Ghatkesar@tudelft.nl

ABSTRACT

Current wafer-scale fabrication methods for graphene-based electronics and sensors involve the transfer of single-layer graphene by a support polymer. This often leaves some polymer residue on the graphene, which can strongly impact its electronic, thermal, and mechanical resonance properties. To assess the cleanliness of graphene fabrication methods, it is thus of considerable interest to quantify the amount of contamination on top of the graphene. Here, we present a methodology for the direct measurement of the mass of the graphene sheet using quartz crystal microbalances (QCMs). By monitoring the QCM resonance frequency during removal of graphene in an oxygen plasma, the total mass of the graphene and contamination is determined with sub-graphene-monolayer accuracy. Since the etch-rate of the contamination is higher than that of graphene, quantitative measurements of the mass of contaminants below, on top, and between graphene layers are obtained. We find that polymer-based dry transfer methods can increase the mass of a graphene sheet by a factor of 10. The presented mass measurement method is conceptually straightforward to interpret and can be used for standardized testing of graphene transfer procedures in order to improve the quality of graphene devices in future applications.

The remarkable electronic,[1] thermal,[2–4] and mechanical[5] properties of graphene have opened the door for many new electronic devices[6–9] and sensors.[10–17] Fabrication of these devices on a wafer scale often requires transfer of sheets of single-layer graphene grown by chemical vapor deposition (CVD), using a support polymer.[18–21] It is inevitable that this introduces some transfer contamination on top of the graphene,[22,23] significantly impacting the device's electronic,[24–26] thermal,[27,28] or mechanical resonance properties.[6,29–31] Therefore, a simple and accurate test to determine the amount of contamination on top of graphene is needed. Typically, the contamination layers on top of graphene are optically transparent, soft, and relatively thin ($<1\ \mu$m). For these reasons, these layers are difficult to detect by popular characterization techniques such as optical microscopy,[33] Raman spectroscopy,[32] and atomic force microscopy.[34]

Several works have determined the amount of contamination on top of graphene resonators by tracking the resonance frequency shift in response to an out-of-plane force.[6,29–31,35] However, these methods require knowledge of the mechanical properties of the resonator, which vary considerably from device-to-device, impacting the accuracy of resonance-based measurement methods.[36–39] Moreover, these resonance based methods only probe contamination over a small area of the suspended resonator, whereas large lateral variations in the amount of contamination can occur. For assessment of production techniques, it is important to have procedures that ensure low contamination levels over large areas.

Here, we present a method to determine the mass of graphene and of the contamination layers on top of graphene, between graphene double-layers, and below graphene. We employ quartz crystal

microbalances (QCMs), which are piezoelectric quartz crystals that can be brought into resonance by applying an oscillating voltage.[40] QCMs are popular tools to measure growth rates during thin film deposition and in biochemical applications,[41,42] because of their simplicity and high accuracy. This has enabled researchers to monitor changes in graphene's mass due to interfacial processes on the surface.[43,44] In this work, we demonstrate the use of QCMs to determine the mass of graphene itself and contaminants by an *in situ* measurement during oxygen plasma etching. In contrast to mechanical resonance based methods, the proposed method is no longer sensitive to the mechanical properties of the graphene and thus facilitates a direct measurement of the mass and furthermore allows large areas of graphene to be studied.

The sensors consist of AT-cut piezoelectric quartz crystals (Novatech S.r.l. AT10-14-6-UP) between two gold contacts, vibrating at a resonance frequency near 10 MHz. A Piranha solution and oxygen plasma treatment on both sides are used to clean the crystals of all organic contaminants, and no significant organic contamination remains after this process as shown in supplementary material S3. Large sheets of graphene grown by chemical vapor deposition (CVD) are transferred on top of one of the electrodes using a widely used dry transfer method.[18] It is ensured that the graphene sheet fully covers the electrode. A second layer of graphene is transferred on some of the crystals to create double-layer graphene. No attempts are performed to clean the graphene after transfer, since we are interested to see the amount of transfer residue on top of the graphene as a result of this process.

Figure 1(a) shows the experimental protocol to measure the mass of graphene. The crystal with CVD graphene is placed in the plasma chamber. Oxygen plasma etches the graphene and organic residues, which reduces the mass on top of the crystal that results in an increase in the QCM resonance frequency. The resonance frequency of the QCM is continuously monitored during the etching process. Stabilization of the resonance frequency indicates full removal of the graphene and all the organic contaminants from the QCM. The shift in the resonance frequency Δf can be related to the removed mass using the Sauerbrey equation,[40]

$$\Delta f = -C\rho h, \tag{1}$$

where ρ is the density, h is the thickness of the material on top of the QCM, and the constant C is given by the properties of the quartz crystal,

$$C = \frac{2}{\sqrt{\rho_q \mu_q}} f_0^2, \tag{2}$$

where ρ_q is the density of quartz, μ_q the shear modulus, and $f_0 = 10$ MHz the unloaded resonance frequency of the crystal. For the crystals used in this work, a single monolayer of graphene with a mass density of $\rho h_{\text{graphene}} = 0.76$ mg/m^2 corresponds to a theoretical resonance frequency shift of 17.19 Hz. Throughout this work, we will often express the mass per unit square or frequency shift in units of equivalent monolayers of graphene.

Figure 1(b) shows the experimental setup to measure the resonance frequency of the crystal during etching. We use a reactive ion etcher (Leybold Hereaus Fluor F2) in a class 10000 (ISO7) cleanroom as the plasma chamber. A blind vacuum flange is adapted to create electrical feedthroughs to the chamber and connected to a KF-40 port on the plasma chamber. A vector network analyzer (VNA) interrogates the resonance frequency of the membrane by a transmission measurement. Alternatively, one can use a commercially available oscillator circuit as shown in supplementary material S1. However, the

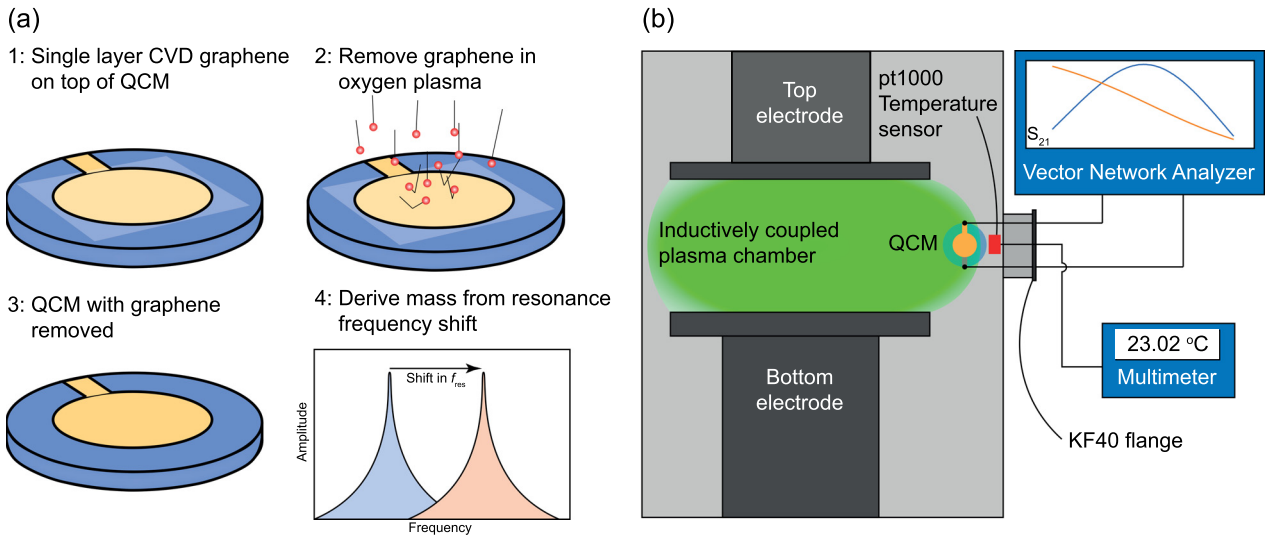

FIG. 1. (a) Experimental procedure to measure the mass of graphene using the quartz crystal microbalance (QCM). The measurement starts with a QCM with a sheet of CVD graphene covering one of the electrodes. The oxygen plasma etches away the graphene and any contaminants until the etching stops. Continuous monitoring of the resonance frequency of the crystal allows one to determine the mass that has been removed by the plasma. (b) Experimental setup to determine the mass of graphene during plasma etching. The QCM and temperature sensor are mounted on a KF40 flange with electrical feedthroughs to an ICP etching chamber. Outside the vacuum chamber, the oscillator circuit processes and conditions the signal from the QCM which is then readout using a frequency counter. A platinum resistor pt1000 thermometer determines the temperature near the QCM.

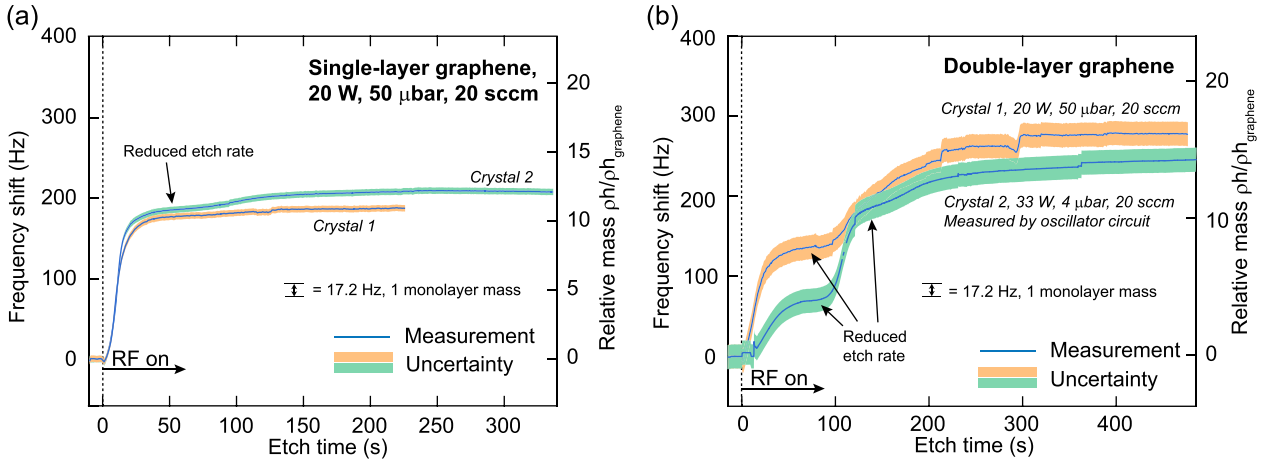

FIG. 2. (a) Frequency shift as a function of etch time for two crystals covered by single layer graphene. At time 0, the oxygen plasma is switched on. Both crystals show an initial high etch rate which rapidly decreases after ∼20 s, followed by a slight increase until the frequency settles. The uncertainty bar is determined by (1) the temperature dependence of the frequency, (2) a small jump in frequency when the RF power is switched on, and (3) the occurrence of sudden jumps in the frequency (see the supplementary material). The total uncertainty is determined to be 7 Hz. (b) Frequency shift for two crystals covered with double-layer graphene. These crystals show a striking decrease in the etching rate, after which the etching rapidly increases again. At approximately 130 s, crystal 2 features a second decrease in the etch rate. The uncertainty is larger with respect to the single-layer devices due to the more frequent occurrence of jumps in the frequency.

VNA produces the best results as it is not sensitive to the interference from the RF plasma at 13.56 MHz—the homodyne detection scheme rejects these frequencies. The oscillator circuit, on the other hand, will often lose lock on the mechanical resonance frequency when the plasma ignites, eliminating measurement data during the etching process (see supplementary material S3). A pt-1000 temperature sensor is placed in the chamber near the crystal to monitor the temperature, because this affects the resonance frequency. The uncertainty in the resonance frequency is determined by three factors, as shown in supplementary material S2: first, the frequency dependence of the crystal on temperature, which is characterized in a subsequent measurement; second, the occurrence of a small (∼3 Hz) jump when the RF power is switched on; and third, the occurrence of random frequency jumps during the measurements which possibly occur due to spurious modes.

Figure 2 shows the resonance frequency of four graphene-covered crystals as a function of the etch time in an oxygen plasma. Crystals covered with single-layer graphene are shown in Fig. 2(a). After the plasma is switched on, the resonance frequency rapidly increases which indicates the removal of mass from the crystal. We observe that after approximately 20 s, the etch rate decreases considerably. After some time, however, the etch rate slightly increases again before the frequency stabilizes. In crystal 1, this corresponds roughly to a monolayer of graphene being etched, while in crystal 2, more mass is removed in this slower regime. A total mass corresponding to 10.8 ± 0.4 layers of graphene is removed from crystal 1, while a total of 12.2 ± 0.4 layers was removed from crystal 2. The total uncertainty of these measurements is determined to be 7 Hz, thus achieving sub-monolayer accuracy in the mass.

The results on the stacked double layers of graphene are shown in Fig. 2(b). Similar to the case of the single-layer graphene, the etching slows down considerably after approximately 40 to 50 s. After this, the etching rate increases significantly. In crystal 2, a second decrease in the etching rate is observed at approximately 130 s of etching time. Later, the etching rate increases again and finally stops. In crystal 1, this second decrease in the etching rate is less prominent due to spurious frequency jumps near 200 s and 300 s. A total mass corresponding to 16.0 ± 1.1 monolayers of graphene is removed from crystal 1, while 14.0 ± 1.1 equivalent monolayers are removed from crystal 2. The more frequent occurrence of random jumps during the measurements of these crystals causes a higher uncertainty compared to the single-layer crystals. Possible causes of the random jumps are outlined in supplementary material S2.

The total etched mass of all the crystals used in this work is shown in Table I. The remaining etching curves that are not shown in Fig. 2 are given in supplementary material S3. For the double layer crystals (DLG), we etch away on average an equivalent mass of 16.7 monolayers of graphene, while for the single layers (SLG), we etch away 11.8 layers of graphene.

We first discuss the observed variation in the etch rate, in particular, the slow etching regimes in the double-layer crystals. By comparing the single layer and double layer crystals in Fig. 2, we conclude that the slower etch rate can be attributed to the graphene, since the double

TABLE I. Measured mass per unit square ρh divided by the theoretical mass of graphene $\rho h_{\text{graphene}} = 0.76$ mg/m^2. The SLG column shows single layer graphene crystals and the DLG column double layer graphene. Three crystals (†) were measured by the VNA, and the remainder (‡) were measured by the oscillator circuit.

Crystal	SLG $\rho h/\rho h_{\text{graphene}}$	Crystal	DLG $\rho h/\rho h_{\text{graphene}}$
1	$12.2^\dagger$	1	$16.0^\dagger$
2	$10.8^\dagger$	2	$14.0^\ddagger$
3	$10.1^\ddagger$	3	$19.7^\ddagger$
4	$14.0^\ddagger$	4	$19.2^\ddagger$
5		5	$14.5^\ddagger$

layer crystals typically show a second decrease in the etching rate. The results thus show that the graphene etching rate is much slower than the contamination. From the data with SLG in Fig. 2(a), we conclude that most of the contamination is present on the top side of the graphene since initially most of the mass is removed, and after the etching slows down, it does not increase again. This makes transfer residues from the polymer a likely source of contamination, which is supported by further measurements on crystals covered by only polymer (without graphene), see supplementary material S3. On Crystal 2 with SLG, significantly more mass (approximately 1.5 equivalent graphene monolayers) is removed in the slow etching regime, which might indicate the presence of contamination underneath the graphene. Possible sources of contamination underneath graphene could be water which is known to accumulate between graphene and the substrate,[45] or insufficient cleaning of organic contaminants from the QCM before transfer. In supplementary material S3, we show a measurement at a much lower plasma power of 4 W. At this power, graphene was not fully removed but rather oxidized as shown by Raman spectroscopy, confirming the slow etching rate of graphene with regard to the contamination.

The measurements of double layer graphene crystals in Fig. 2(b) provide further evidence that the slower etch rate can be attributed to the graphene. One interpretation of the data is that the etching of the first graphene layer causes a significant decrease in the etching rate after 40 s, and the less-prominent second decrease can be attributed to the second graphene layer. Since the etching rate significantly increases after slowing down, we conclude that the stacking of these layers effectively results (from bottom to top) in a graphene-residue-graphene-residue stack. While the first region with a slow etch rate shows a relatively sharp decrease in the etching rate, the second slow regime is considerably smoother. This may be due to lateral nonuniformities in the etch rate or contamination thickness, which result in variations in the time when the second graphene layer is reached and etched. One striking observation is that the addition of the second graphene layer increases the mass by only ~40%, instead of doubling the mass. From the experiments (Fig. 2), it appears that the additional mass can be attributed to the top contamination layer of the single layer graphene, while this layer is significantly thinner in the double-layer crystals. The underlying cause of this observation is currently unknown.

The method presented here can be used in several future technological applications. For example, the frequency range of tunable oscillators[7,46,47] and the responsivity of resonating pressure sensors[14–16,35] are significantly impacted by the mass-per-unit-square of the device. The method is also a useful technique to determine the presence of contamination. The electron mobility of graphene, for example, is significantly impacted by contaminants.[24–26,48,49] Graphene has also been proposed as heat spreaders for thermal management in electronic circuits,[50] but contaminated samples also show a significantly lower thermal conductivity.[27,28] For upscaling electronic and thermal graphene applications to the wafer scale, the proposed QCM method can be used to select the best transfer technique to produce high-quality graphene devices. Furthermore, the QCM method no longer requires the fabrication and testing of devices to optimize the transfer procedure,[24–26,48,49] which simplifies the procedure and improves the throughput of the optimization process. The QCM method thus enables large-scale quality control of graphene sheets. Moreover, since graphene etches much slower than the contamination, the technique can discriminate between the amount of contamination underneath and on top of the graphene.

For research, the method is useful to study the mass of wrinkled graphene membranes to reveal their hidden area,[51] for example, graphene transferred on smooth or rough substrates. Furthermore, the QCM measurement can be a corroboration to the number of layers revealed by Raman spectroscopy.[32] In particular, the method is accurate enough to count the number of layers on few-layer graphene samples, in the regime where this is difficult to achieve with Raman spectroscopy. Moreover, in heterostructures or other stacks of multilayer 2D materials, the QCMs are useful to reveal the presence of trapped residual materials, which can hamper the interlayer coupling that gives these stacks their favorable properties.

To conclude, we present a method to determine the mass-per-unit-square and etch rate of CVD-grown graphene sheets using quartz crystal microbalances. This is achieved by etching graphene on a QCM in oxygen plasma and measuring the resonance frequency of the crystal *in situ*. We find that by using a widely used dry transfer method, the mass of the single-layer graphene sheet is observed to be ten times higher than the theoretical mass of graphene. The time-dependence of the etching rate shows that most of the contamination is on top of the graphene. The method is useful for quality control of large sheets of graphene for future sensing, electronic, and thermal applications.

See the supplementary material for (S1) further information on the measurement setup using the commercially available oscillator circuit; (S2) determination of the uncertainty in the frequency shift; and (S3) additional measurement results, including more crystals included in Table I, measurements using low RF power, measurements on bare crystals, and measurements on polymer-covered crystals without graphene.

The authors thank Applied Nanolayers B.V. for supply and transfer of the single-layer graphene and Hugo Solera Licona for help with cleaning the crystals. This work is part of the research programme Integrated Graphene Pressure Sensors (IGPS) with Project No. 13307 which is financed by the Netherlands Organisation for Scientific Research (NWO). The research leading to these results also received funding from the European Union's Horizon 2020 research and innovation programme under Grant Agreement No. 785219 Graphene Flagship. The authors acknowledge support from the Australian Research Council Centre of Excellence in Exciton Science (No. CE170100026) and the Australian Research Council Grants Scheme.

REFERENCES

[1]A. C. Neto, F. Guinea, N. Peres, K. S. Novoselov, and A. K. Geim, Rev. Mod. Phys. **81**, 109 (2009).
[2]A. A. Balandin, S. Ghosh, W. Bao, I. Calizo, D. Teweldebrhan, F. Miao, and C. N. Lau, Nano Lett. **8**, 902 (2008).
[3]E. Pop, V. Varshney, and A. K. Roy, MRS Bull. **37**, 1273 (2012).
[4]R. J. Dolleman, S. Houri, D. Davidovikj, S. J. Cartamil-Bueno, Y. M. Blanter, H. S. van der Zant, and P. G. Steeneken, Phys. Rev. B **96**, 165421 (2017).
[5]C. Lee, X. Wei, J. W. Kysar, and J. Hone, Science **321**, 385 (2008).
[6]X. Song, M. Oksanen, M. A. Sillanpaa, H. Craighead, J. Parpia, and P. J. Hakonen, Nano Lett. **12**, 198 (2012).
[7]C. Chen, S. Lee, V. V. Deshpande, G.-H. Lee, M. Lekas, K. Shepard, and J. Hone, Nat. Nanotechnol. **8**, 923 (2013).

[8]M. C. Lemme, T. J. Echtermeyer, M. Baus, and H. Kurz, IEEE Electron Device Lett. **28**, 282 (2007).
[9]S. J. Cartamil-Bueno, D. Davidovikj, A. Centeno, A. Zurutuza, H. S. J. van der Zant, P. G. Steeneken, and S. Houri, Nat. Commun. **9**, 4837 (2018).
[10]J. Dauber, A. A. Sagade, M. Oellers, K. Watanabe, T. Taniguchi, D. Neumaier, and C. Stampfer, Appl. Phys. Lett. **106**, 193501 (2015).
[11]A. D. Smith, K. Elgammal, X. Fan, M. C. Lemme, A. Delin, M. Råsander, L. Bergqvist, S. Schröder, A. C. Fischer, F. Niklaus *et al.*, RSC Adv. **7**, 22329 (2017).
[12]F. Ricciardella, S. Vollebregt, T. Polichetti, M. Miscuglio, B. Alfano, M. L. Miglietta, E. Massera, G. Di Francia, and P. M. Sarro, Nanoscale **9**, 6085 (2017).
[13]A. D. Smith, S. Vaziri, F. Niklaus, A. C. Fischer, M. Sterner, A. Delin, M. Östling, and M. C. Lemme, Solid-State Electron. **88**, 89 (2013).
[14]R. J. Dolleman, D. Davidovikj, S. J. Cartamil-Bueno, H. S. van der Zant, and P. G. Steeneken, Nano Lett. **16**, 568 (2016).
[15]R. J. Dolleman, S. J. Cartamil-Bueno, H. S. J. van der Zant, and P. G. Steeneken, 2D Mater. **4**, 011002 (2017).
[16]S. Vollebregt, R. J. Dolleman, H. S. J. van der Zant, P. G. Steeneken, and P. M. Sarro, in *Transducers 2017, The 19th International Conference on Solid-State Sensors, Actuators and Microsystems* (IEEE, 2017), pp. 770–773.
[17]D. Davidovikj, P. H. Scheepers, H. S. J. van der Zant, and P. G. Steeneken, ACS Appl. Mater. Interfaces **9**, 43205 (2017).
[18]J. W. Suk, A. Kitt, C. W. Magnuson, Y. Hao, S. Ahmed, J. An, A. K. Swan, B. B. Goldberg, and R. S. Ruoff, ACS Nano **5**, 6916 (2011).
[19]X. Li, Y. Zhu, W. Cai, M. Borysiak, B. Han, D. Chen, R. D. Piner, L. Colombo, and R. S. Ruoff, Nano Lett. **9**, 4359 (2009).
[20]Y. Lee, S. Bae, H. Jang, S. Jang, S.-E. Zhu, S. H. Sim, Y. I. Song, B. H. Hong, and J.-H. Ahn, Nano Lett. **10**, 490 (2010).
[21]X.-D. Chen, Z.-B. Liu, C.-Y. Zheng, F. Xing, X.-Q. Yan, Y. Chen, and J.-G. Tian, Carbon **56**, 271 (2013).
[22]M. Her, R. Beams, and L. Novotny, Phys. Lett. A **377**, 1455 (2013).
[23]Y.-C. Lin, C.-C. Lu, C.-H. Yeh, C. Jin, K. Suenaga, and P.-W. Chiu, Nano Lett. **12**, 414 (2012).
[24]A. Pirkle, J. Chan, A. Venugopal, D. Hinojos, C. Magnuson, S. McDonnell, L. Colombo, E. Vogel, R. Ruoff, and R. Wallace, Appl. Phys. Lett. **99**, 122108 (2011).
[25]J. W. Suk, W. H. Lee, J. Lee, H. Chou, R. D. Piner, Y. Hao, D. Akinwande, and R. S. Ruoff, Nano Lett. **13**, 1462 (2013).
[26]J. Chan, A. Venugopal, A. Pirkle, S. McDonnell, D. Hinojos, C. W. Magnuson, R. S. Ruoff, L. Colombo, R. M. Wallace, and E. M. Vogel, ACS Nano **6**, 3224 (2012).
[27]M. T. Pettes, I. Jo, Z. Yao, and L. Shi, Nano Lett. **11**, 1195 (2011).
[28]I. Jo, M. T. Pettes, L. Lindsay, E. Ou, A. Weathers, A. L. Moore, Z. Yao, and L. Shi, AIP Adv. **5**, 053206 (2015).
[29]V. Singh, S. Sengupta, H. S. Solanki, R. Dhall, A. Allain, S. Dhara, P. Pant, and M. M. Deshmukh, Nanotechnology **21**, 165204 (2010).
[30]R. A. Barton, I. R. Storch, V. P. Adiga, R. Sakakibara, B. R. Cipriany, B. Ilic, S. P. Wang, P. Ong, P. L. McEuen, J. M. Parpia, and H. G. Craighead, Nano Lett. **12**, 4681 (2012).
[31]C. Chen, S. Rosenblatt, K. I. Bolotin, W. Kalb, P. Kim, I. Kymissis, H. L. Stormer, T. F. Heinz, and J. Hone, Nat. Nanotechnol. **4**, 861 (2009).
[32]A. Ferrari, J. Meyer, V. Scardaci, C. Casiraghi, M. Lazzeri, F. Mauri, S. Piscanec, D. Jiang, K. Novoselov, S. Roth, and A. Geim, Phys. Rev. Lett. **97**, 187401 (2006).
[33]P. Blake, E. W. Hill, A. Castro Neto, K. S. Novoselov, D. Jiang, R. Yang, T. J. Booth, and A. Geim, Appl. Phys. Lett. **91**, 063124 (2007).
[34]P. Nemes-Incze, Z. Osváth, K. Kamarás, and L. Biró, Carbon **46**, 1435 (2008).
[35]J. S. Bunch, S. S. Verbridge, J. S. Alden, A. M. Van Der Zande, J. M. Parpia, H. G. Craighead, and P. L. McEuen, Nano Lett. **8**, 2458 (2008).
[36]D. Davidovikj, F. Alijani, S. J. Cartamil-Bueno, H. S. J. van der Zant, M. Amabili, and P. G. Steeneken, Nat. Commun. **8**, 1253 (2017).
[37]R. J. Nicholl, H. J. Conley, N. V. Lavrik, I. Vlassiouk, Y. S. Puzyrev, V. P. Sreenivas, S. T. Pantelides, and K. I. Bolotin, Nat. Commun. **6**, 8789 (2015).
[38]J.-U. Lee, D. Yoon, and H. Cheong, Nano Lett. **12**, 4444 (2012).
[39]C. S. Ruiz-Vargas, H. L. Zhuang, P. Y. Huang, A. M. Van Der Zande, S. Garg, P. L. McEuen, D. A. Muller, R. G. Hennig, and J. Park, Nano Lett. **11**, 2259 (2011).
[40]G. Sauerbrey, Z. Phys. **155**, 206 (1959).
[41]C. O'Sullivan and G. Guilbault, Biosens. Bioelectron. **14**, 663 (1999).
[42]D. A. Buttry and M. D. Ward, Chem. Rev. **92**, 1355 (1992).
[43]N. Kakenov, O. Balci, O. Salihoglu, S. H. Hur, S. Balci, and C. Kocabas, Appl. Phys. Lett. **109**, 053105 (2016).
[44]V. Van Quang, V. N. Hung, V. N. Phan, T. Q. Huy, and N. Van Quy, Thin Solid Films **568**, 6 (2014).
[45]Q. Li, J. Song, F. Besenbacher, and M. Dong, Acc. Chem. Res. **48**, 119 (2015).
[46]D. Davidovikj, M. Poot, S. J. Cartamil-Bueno, H. S. van der Zant, and P. G. Steeneken, Nano Lett. **18**, 2852 (2018).
[47]F. Ye, J. Lee, and P. X.-L. Feng, in *2017 IEEE 30th International Conference on Micro Electro Mechanical Systems (MEMS)* (IEEE, 2017), pp. 68–71.
[48]A. Goossens, V. Calado, A. Barreiro, K. Watanabe, T. Taniguchi, and L. Vandersypen, Appl. Phys. Lett. **100**, 073110 (2012).
[49]J. Moser, A. Barreiro, and A. Bachtold, Appl. Phys. Lett. **91**, 163513 (2007).
[50]S. Ghosh, I. Calizo, D. Teweldebrhan, E. Pokatilov, D. Nika, A. Balandin, W. Bao, F. Miao, and C. N. Lau, Appl. Phys. Lett. **92**, 151911 (2008).
[51]R. J. T. Nicholl, N. V. Lavrik, I. Vlassiouk, B. R. Srijanto, and K. I. Bolotin, Phys. Rev. Lett. **118**, 266101 (2017).